

Proton-spin-lattice relaxation in the antiferromagnetic state of $\text{CsMnCl}_3 \cdot 2\text{H}_2\text{O}$

H. Nishihara, W. J. M. de Jonge, and T. de Neef

Department of Physics, Eindhoven University of Technology, Eindhoven, The Netherlands

(Received 18 February 1975)

The spin-lattice relaxation times of protons in the nearly one-dimensional Heisenberg system $\text{CsMnCl}_3 \cdot 2\text{H}_2\text{O}$ were measured between 1.1 and 3.9 K in the antiferromagnetic state. From the comparison of the ratio of the relaxation rates of two nonequivalent protons with the calculated ratio, it was concluded that the two-magnon process dominates at low temperatures and the exchange-enhanced three-magnon process at high temperatures. A quantitative calculation of these contributions, without the restriction of a small- k approximation, based on the values for the exchange constants available in the literature, gives a fair agreement with the experimental results. The relaxation time is very sensitive to the interchain coupling and a fitting procedure to our experimental data yields an interchain coupling of $(5 \pm 1)\%$ of the intrachain coupling.

I. INTRODUCTION

Nuclear-spin-lattice relaxation in the ordered state of magnetic insulators has been the subject of a number of experimental as well as theoretical publications.¹⁻¹⁰ A theoretical review of the most important processes has been given by Beeman and Pincus.⁸ In the majority of papers a qualitative agreement with the behavior of one or more dominating processes was concluded. Quantitative agreement between the experimental data and the calculated relaxation rates has been obtained in only a few cases. The two-magnon (Raman) process, which is allowed if the interaction contains terms like I^+S^z , was shown to be effective in the relaxation of ^{19}F in the three-dimensional Heisenberg antiferromagnet MnF_2 .⁵ In the two-dimensional ferromagnetic layers in CrCl_3 , the relaxation of ^{53}Cr was found to be in quantitative agreement with the exchange-enhanced three-magnon process.⁷

Recently, the spin dynamics of the nearly-one-dimensional Heisenberg system $(\text{CH}_3)_4\text{N MnCl}_3$ has received considerable attention.^{11,12} The relaxation of the protons in the *paramagnetic* state was interpreted on the basis of a direct process, which was possible because of the vanishingly small energy gap and the characteristic one-dimensional dispersion relation.¹¹ In the *ordered* state of such a system one might anticipate a dramatic influence of the small interchain interactions on the density of states, because in the (nonphysical) limit of the (ordered) purely one-dimensional case the density of states diverges in the origin of the \vec{k} space.

In view of this we thought it worthwhile to study the relaxation mechanism of the nearly-one-dimensional antiferromagnet $\text{CsMnCl}_3 \cdot 2\text{H}_2\text{O}$ in the *ordered* state. This system is particularly attractive because its crystallographic and mag-

netic properties, including the spin-wave excitations of the electron system, are well established, as will be reviewed in Sec. II. Moreover, the presence of two magnetically nonequivalent hydrogen nuclei, coupled to the electron-spin system through dipole-dipole interaction, enabled us to apply a new technique of assignment of the relaxation mechanisms, which uses the ratio of the relaxation times of the two inequivalent nuclei. This will be discussed in Sec. III together with the theoretical treatment of the relaxation processes. In Sec. IV the results will be summarized and discussed.

II. CRYSTAL STRUCTURE AND MAGNETIC PROPERTIES OF $\text{CsMnCl}_3 \cdot 2\text{H}_2\text{O}$

The crystallographic structure of $\text{CsMnCl}_3 \cdot 2\text{H}_2\text{O}$ is orthorhombic with space-group $Pcca$.¹³ The unit cell contains four molecular units and has the dimensions $a = 9.060$, $b = 7.285$, and $c = 11.455$ Å. A detailed structure is shown in Fig. 1(a), where H(1) and H(2) mark the two inequivalent hydrogen sites in the unit cell. Slightly staggered chains $-\text{Cl}^- - \text{Mn}^{2+} - \text{Cl}^- - \text{Mn}^{2+} -$ extend in the a direction, the Cl^- ions providing the intrachain superexchange coupling between the Mn^{2+} spins. The Mn^{2+} ions on neighboring chains are linked by indirect paths involving at least two intermediate atoms. $\text{CsMnCl}_3 \cdot 2\text{H}_2\text{O}$ exhibits three-dimensional long-range order below $T_N = 4.89$ K,^{14,15} and the spin structure is shown in Fig. 1(b).¹⁵ The magnetic space group is $P_{2b}c'ca'$ and the preferred direction of the spin alignment is the b axis. The paths of the exchange interactions are also depicted, J_1 is the intrachain interaction and J_2, J_3 are interchain interactions.

The pronounced one-dimensional antiferromagnetic character was observed in many experiments. Inelastic neutron scattering on $\text{CsMnCl}_3 \cdot 2\text{D}_2\text{O}$

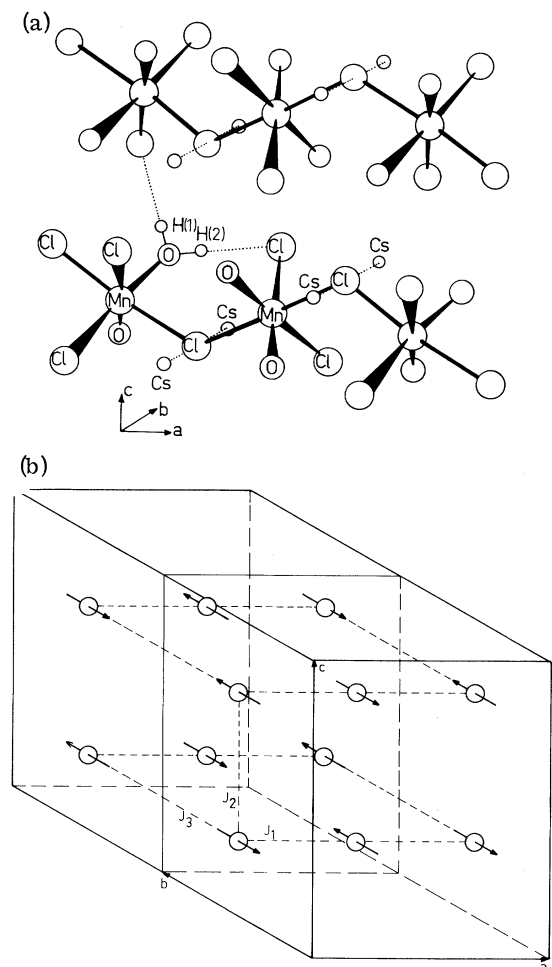


FIG. 1. (a) Schematic crystal structure of $\text{CsMnCl}_3 \cdot 2\text{H}_2\text{O}$. A set of nonequivalent protons H(1) and H(2) is shown. (b) Spin structure in $\text{CsMnCl}_3 \cdot 2\text{H}_2\text{O}$. J_1 denotes the intrachain exchange interaction along the a axis, J_2 and J_3 are the interchain interactions.

revealed that the spin-wave spectrum below T_N is highly anisotropic and the short-wavelength magnon modes in the chains persist even at $2T_N$.¹⁶ The line shape of the paramagnetic-electron-spin resonance and the proton relaxation time in the paramagnetic state were also explained with a nearly-one-dimensional Heisenberg model,¹⁷⁻¹⁹ but there is a difference of a factor of 5 among the estimated magnitudes of the interchain couplings obtained from different experimental techniques, as tabulated in Table I. The energy gap of the spin-wave spectrum at zero wave vector $\epsilon_0/k = 1.7$ K at $T = 4.2$ K and 2.2 K at $T = 1.5$ K,^{16,20} and the two values are consistent if the energy gap renormalizes proportionally to the sublattice magnetization.¹⁶

III. THEORY

Theoretical treatments on nuclear-spin-lattice relaxation in three-dimensional ferromagnetic or antiferromagnetic insulators can be found in a number of publications.²⁻¹⁰ In this section we will restrict ourselves to the characteristics of a nearly-one-dimensional case, a situation which applies to $\text{CsMnCl}_3 \cdot 2\text{H}_2\text{O}$. The available experimental data show that the spin-wave spectrum has an energy gap and that the spin structure is collinear. The interactions between the electron-spin system and the nuclear spins on the hydrogens of the water molecules are mainly dipolar. In that case the relaxation processes which can be effective are the two-magnon process and the exchange-enhanced three-magnon process. We will treat these processes in Secs. III B and III C together with the spin-wave spectrum and the density of states. Apart from the temperature dependence of the anisotropy energy gap in the spin-wave spectrum and the magnon-magnon interaction perturbation used in the calculations of the exchange-enhanced three-magnon process, this treatment is based on linear spin-wave theory and no other renormalization effects are considered. This approximation is certainly correct as far as the magnon energies associated with wave propagating in the chain direction is concerned. Skalyo *et al.*¹⁶ already showed that the energy renormalization for this branch is only detectable far above T_N . For the out-of-chain excitations, however, a 10% energy normalization for the zone-boundary magnons was observed. The influence of this renormalization on the calculated magnon density and relaxation rates may be qualitatively estimated from the order of the change in these quantities when the interchain exchange parameters are slightly altered, as will be shown.

A. Spin-wave spectrum

We assume that the electron-spin system in $\text{CsMnCl}_3 \cdot 2\text{H}_2\text{O}$ can be described by the following Hamiltonian:

$$\mathcal{H} = -2 \sum_{\langle l, m \rangle} J_{lm} (\tilde{S}_l \cdot \tilde{S}_m) - g \mu_B H_A \left(\sum_l S_l^z - \sum_m S_m^z \right), \quad (1)$$

where the indices l, m refer to the plus and minus sublattices, respectively, g is the g factor, μ_B is the Bohr magneton, and H_A is the anisotropy field. The exchange constant J_{lm} for a nearest-neighbor pair $\langle l, m \rangle$ in the a, b , and c directions is different and the slight zigzag of the chains will be ignored.¹⁶

TABLE I. Values of exchange constants in $\text{CsMnCl}_3 \cdot 2\text{H}_2\text{O}$ obtained from different experimental techniques.

| Experiment | Exchange constants (K) | Reference |
|-------------------------------|---|-----------|
| Paramagnetic susceptibility | $J_1/\kappa = -3.0$ | 22 |
| Neutron diffraction | $J_1/\kappa = -3.53$ $J_2 + J_3 = 0.7 \times 10^{-2} J_1$ | 16 |
| Line shift of ESR | $J_1/\kappa = -3.57$ | 21 |
| Perpendicular susceptibility | $J_1/\kappa = -3.39$ | 23 |
| Specific heat | $J_1/\kappa = -3.3$ | 24 |
| Line shape of ESR | between $ J_2 = J_3 = 2 \times 10^{-2} J_1 $ and $ J_2 = 100 J_3 = 2.6 \times 10^{-2} J_1 $ | 17 |
| NMR in the paramagnetic state | $ J_2 = 3.5 \times 10^{-2} J_1 \gg J_3 $ | 19 |

After diagonalization the spin-wave energy can be expressed as

$$\epsilon(\vec{k}) = \{\epsilon_m^2 - [2SJ(\vec{k})]^2\}^{1/2}, \quad (2)$$

where

$$\epsilon_m = 4S(-J_1 - J_2 - J_3) + g\mu_B H_A,$$

$$J(\vec{k}) = \sum_{\delta} J_{\delta} e^{-i(\vec{k} \cdot \vec{\delta})}$$

$$= 2(J_1 \cos \frac{1}{2} k_x a + J_2 \cos \frac{1}{2} k_y c + J_3 \cos k_z b),$$

and ϵ_m equals the maximum energy of the spin-wave spectrum. The minimum energy (energy gap) ϵ_0 is given by $\epsilon(k=0)$ and we have taken this as a temperature-dependent parameter instead of H_A . The two modes of spin waves are degenerate in zero external field. This dispersion relation is essentially different from that in the paramagnetic state¹¹ due to the change of magnetic symmetry and the existence of long-range correlations, in particular, perpendicular to the chains.

B. Two-magnon process

The hyperfine interaction between the electron-spin system and a proton is assumed to be purely

dipolar with the Hamiltonian for the j th proton

$$\begin{aligned} \mathcal{H}_N = & -\gamma_N \hbar \vec{I}_j \cdot \left(\vec{H}_0 - g\mu_B \sum_l \gamma_l^{-3} \right. \\ & \times [\vec{S}_l - 3\vec{r}_l(\vec{r}_l \cdot \vec{S}_l)\gamma_l^{-2}] \\ & \left. - g\mu_B \sum_m \gamma_m^{-3} [\vec{S}_m - 3\vec{r}_m(\vec{r}_m \cdot \vec{S}_m)\gamma_m^{-2}] \right), \quad (3) \end{aligned}$$

where γ_N is the gyromagnetic ratio of the proton, \vec{H}_0 is the external field, and \vec{r}_l is the position vector of the l th electron spin with respect to the position of the j th proton.

The calculation of the transition probability for the process in which a spin wave of wave vector \vec{k} is scattered to that of \vec{k}' accompanied by a nuclear-spin flip gives the relaxation rate of the two-magnon process for the j th proton²:

$$\frac{1}{T_1^{(2)}(j)} = \frac{2\pi}{\hbar} (g\mu_B \gamma_N \hbar)^2 G_2(j) I_2. \quad (4)$$

In this expression $G_2(j)$ is a "geometrical factor" which is the part of the matrix element that depends only on the difference of the quantization axes of the electron spins and the nuclear spin \vec{I}_j and on the geometrical positions of the electron spins with respect to the position of the j th proton. It can be written as^{2,10,25}

$$\begin{aligned} G_2(j) = & \sum_l \gamma_l^{-6} |h_l|^2 + \sum_m \gamma_m^{-6} |h_m|^2, \\ |h_l|^2 = & \frac{1}{4} \sin^2 \theta [(1 - 3 \cos^2 \theta_l)^2 - 9 \cos^2(\phi - \phi_l) \sin^2 \theta_l \cos^2 \theta_l] + \frac{3}{4} \sin^2 \theta_l \cos^2 \theta_l \\ & + \frac{3}{2} \sin \theta \cos \theta (1 - 3 \cos^2 \theta_l) \cos(\phi - \phi_l) \sin \theta_l \cos \theta_l, \quad (5) \end{aligned}$$

where θ_i , ϕ_i are the angular parts of the spherical coordinates of \vec{r}_i , and θ , ϕ those of the total field vector acting on the j th proton. Both are measured from a coordinate axis fixed to the crystallographic axis. It should be noted that $G_2(j)$ is not proportional to $\sin^2\theta$ and depends on $\phi - \phi_i$. This is not the case when one deals with hyperfine interactions of the type $A\vec{I} \cdot \vec{S}$.

I_2 is an integral which depends on the temperature and the spin-wave dispersion and is given by

$$I_2 = \int_{\epsilon_0}^{\epsilon_m} \frac{e^{\epsilon/\kappa T}}{(e^{\epsilon/\kappa T} - 1)^2} [(\epsilon_m/\epsilon)^2 + 1] [N(\epsilon)]^2 d\epsilon. \quad (6)$$

In this expression ϵ_0 and ϵ_m are the minimum and maximum spin-wave energy, κ is the Boltzmann constant, $N(\epsilon)$ is the normalized density of states:

$$N(\epsilon) = \frac{1}{N_s} \frac{V}{(2\pi)^3} \int \int \frac{dS_{\vec{k}}}{|\nabla_{\vec{k}} \epsilon(\vec{k})|}, \quad (7)$$

which satisfies

$$\int_{\epsilon_0}^{\epsilon_m} N(\epsilon) d\epsilon = 1. \quad (8)$$

N_s is the total number of spins in each sublattice or the total number of states in each branch of the spin wave and V is the volume of the sample. In the actual calculation of I_2 , the small- k approximation has widely been used. However, it cannot be applied to a nearly-one-dimensional case because the density of states $N(\epsilon)$ exhibits a peak in the small-energy region which is of great influence and cannot be produced with the small- k approximation. In fact, $N(\epsilon_0)$ diverges in a purely one-dimensional case. This forced us to calculate $N(\epsilon)$ numerically for given sets of exchange parameters. Examples are shown in Fig. 2 together with the density of the purely one-dimensional case, which can be written as

$$N(\epsilon) = (2/\pi)\epsilon(\epsilon^2 - \epsilon_0^2)^{-1/2}(\epsilon_m^2 - \epsilon^2)^{-1/2}. \quad (9)$$

and that of the small- k approximation²⁶

$$N(\epsilon) = (8\sqrt{2} \pi^2 S^3)^{-1} (J_1^4 J_2 J_3)^{-1/2} \epsilon_0^{3/2} (\epsilon - \epsilon_0)^{1/2}. \quad (10)$$

The calculated densities have large values in the high-energy region which resemble the density in the purely one-dimensional case. However, the contribution of this part is not significant because of the Bose exponential factor in Eq. (6). In general, one may safely state that whereas ϵ_m in nearly-one-dimensional systems is mainly determined by the strong intrachain interaction and T_N is determined by the interplay of the inter and intrachain interactions, zone-boundary effects in the relaxation times of these systems in the anti-ferromagnetic state ($T < T_N$) will not be significant.

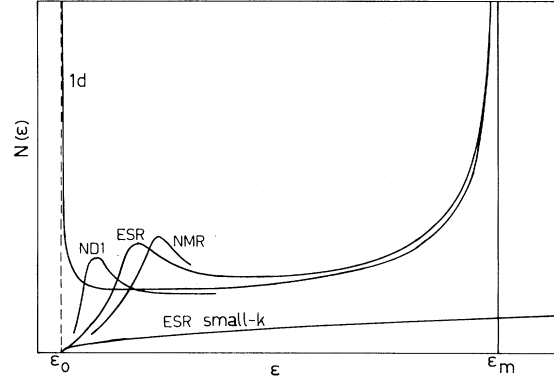


FIG. 2. Examples of the magnon density of states $N(\epsilon)$ vs ϵ for different sets of exchange constants. The labels refer to (see Table I): ESR: $J_1/\kappa = -3.0$ K, $J_2 = J_3 = 2 \times 10^{-2} J_1$. 1d: one-dimensional limit with the same minimum and maximum energies as ESR. ESR, small k : the density in the small- k approximation for ESR. ND1: $J_1/\kappa = -3.53$ K, $J_2 = J_3 = 0.35 \times 10^{-2} J_1$. NMR: $J_1/\kappa = -3.0$ K, $J_2 = 3.5 \times 10^{-2} J_1$, $J_3 = 0$. Only the shape around a peak is depicted for each of the last two cases.

Thus, by measuring the proton relaxation time we are dealing with the low-energy part of the density of states and this strongly depends on the degree of one dimensionality. Information about the interchain coupling can thus be obtained from the absolute value of T_1 . The method of numerical calculation of the density of states used in this paper is sketched in the Appendix.

C. Three-magnon process and its exchange enhancement in $\text{CsMnCl}_3 \cdot 2\text{H}_2\text{O}$

The three-magnon relaxation rate is calculated from the first-order transition probability in which one magnon is annihilated and two are created or two magnons are annihilated and one is created when a nuclear spin flips.^{4,6,8} The relaxation rate for the j th proton in our spin structure is

$$\frac{1}{T_1^{(3)}(j)} = \frac{2\pi}{\hbar} (g \mu_B \gamma_N \hbar)^2 G_3(j) I_3, \quad (11)$$

where $G_3(j)$ is the geometrical factor for the j th proton in the case of the three-magnon process and can be written as^{10,25}

$$G_3(j) = \sum_l r_l^{-6} (|v_l^+|^2 + |v_l^-|^2) + \sum_m r_m^{-6} (|v_m^+|^2 + |v_m^-|^2), \quad (12)$$

with

$$v_i^\pm = \frac{1}{8} [6 \sin \theta \sin \theta_i \cos \theta_i \pm (1 \mp \cos \theta)(1 - 3 \cos^2 \theta_i) e^{-i(\phi - \phi_i)} \mp 3(1 \pm \cos \theta) \sin^2 \theta_i e^{i(\phi - \phi_i)}]. \quad (13)$$

$$I_3 = \frac{3}{16S} N_s^{-3} \sum_{\vec{k}_1} \sum_{\vec{k}_2} \sum_{\vec{k}_3} \frac{\epsilon_m^3}{\epsilon_1 \epsilon_2 \epsilon_3} [\langle n_1 + 1 \rangle \langle n_2 + 1 \rangle \langle n_3 \rangle \delta(\epsilon_1 + \epsilon_2 - \epsilon_3) + \langle n_1 + 1 \rangle \langle n_2 \rangle \langle n_3 \rangle \delta(\epsilon_1 - \epsilon_2 - \epsilon_3)] \quad (14a)$$

$$= \frac{3}{8S} \int_{\epsilon_0}^{\epsilon_m} \int_{\epsilon_0}^{\epsilon_m} \frac{e^{(\epsilon_1 + \epsilon_2)/\kappa T}}{(e^{\epsilon_1/\kappa T} - 1)(e^{\epsilon_2/\kappa T} - 1)(e^{(\epsilon_1 + \epsilon_2)/\kappa T} - 1)} \frac{\epsilon_m^3}{\epsilon_1 \epsilon_2 (\epsilon_1 + \epsilon_2)} N(\epsilon_1) N(\epsilon_2) N(\epsilon_1 + \epsilon_2) d\epsilon_1 d\epsilon_2, \quad (14b)$$

where ϵ_i means $\epsilon(\vec{k}_i)$ and $\langle n_i \rangle$ is the Bose distribution function

$$\langle n_i \rangle = (e^{\epsilon(\vec{k}_i)/\kappa T} - 1)^{-1}. \quad (15)$$

In the derivation of (14) we used the approximation

$$[\epsilon_m/\epsilon(\vec{k})]^2 \gg 1. \quad (16)$$

Especially in the nearly-one-dimensional case this approximation should be quite good as discussed in Sec. III B.

This type of calculation of the three-magnon process has been shown, however, to underestimate the three-magnon process, because there are other transitions that involve identical initial and final states.^{6,8} This process, which is called the exchange-enhanced three-magnon process, is calculated from the probability of second-order

I_3 is a summation over wave vectors or a double integral, which depends on the temperature and the magnon dispersion relation

transitions via the four-magnon terms in the exchange interaction plus the one-magnon terms in the hyperfine interaction. The effect was observed in the ferromagnetic layers in CrCl_3 ,⁷ and was also predicted in the antiferromagnetic case. The prediction based on the Dyson-Mal'ëv representation⁹ was different from the original prediction based on the Holstein-Primakoff formalism.⁸ Here we recalculate the process in the case of dipole-dipole hyperfine interaction and our spin arrangement, using the Holstein-Primakoff formalism which is easier to understand.²⁷

Expanding the Hamiltonian (1) with the spin-wave operators in the Holstein-Primakoff representation and keeping terms down to order S^0 , we obtain the magnon-magnon interaction (or exchange-scattering) term

$$\begin{aligned} \mathcal{H}'_{\text{ex}} = & (2N_S)^{-1} \sum_{\vec{k}_1} \sum_{\vec{k}_2} \sum_{\vec{k}_3} \sum_{\vec{k}_4} \delta(\vec{k}_1 + \vec{k}_2 - \vec{k}_3 - \vec{k}_4) (\frac{1}{2} \epsilon_m)^2 (\epsilon_1 \epsilon_2 \epsilon_3 \epsilon_4)^{-1/2} \\ & \times [2J(\vec{k}_2 - \vec{k}_3) + 2J(\vec{k}_1 - \vec{k}_3) - J(\vec{k}_1) - J(\vec{k}_2) - J(\vec{k}_3) - J(\vec{k}_4)] (\alpha_1^* \alpha_2^* \alpha_3 \alpha_4 - 2\alpha_1^* \beta_2 \alpha_3 \alpha_4 \\ & - 2\alpha_1^* \alpha_2^* \alpha_3 \beta_4^* + 4\alpha_1^* \beta_2 \alpha_3 \beta_4^* - 2\alpha_1^* \beta_2 \beta_3^* \beta_4^* - 2\beta_1 \beta_2 \alpha_3 \beta_4^* + \beta_1 \beta_2 \beta_3^* \beta_4^*), \end{aligned} \quad (17)$$

where α_i , α_i^* , β_i and β_i^* are the creation and annihilation operators of spin waves of wave vectors \vec{k}_i in the α and β branch of the spin-wave spectrum. In the evaluation of (17) the "small-energy" approximation (16) is used. No use has been made of the small- k approximation.

With approximation (16) the one-magnon term of the dipole-dipole hyperfine interaction (3) will be

$$\begin{aligned} \mathcal{H}'_1 = & I'_+ \sum_i \left[v_i^{-3} (-\sqrt{2S} g \mu_B \gamma_N \hbar) N_S^{-1/2} \sum_{\vec{k}} \left(\frac{\epsilon_m}{2\epsilon(\vec{k})} \right)^{1/2} \right. \\ & \left. \times [v_i^+ e^{-i\vec{k} \cdot \vec{r}} (\alpha_{\vec{k}}^* - \beta_{\vec{k}}^*) + v_i^- e^{i\vec{k} \cdot \vec{r}} (\alpha_{\vec{k}} - \beta_{\vec{k}})] \right] \\ & + I'_+ \sum_m (\dots), \end{aligned} \quad (18)$$

where I'_+ is a nuclear-spin operator in the coordinate system whose z' axis is parallel to the total field on the j th proton. Calculation of the second-order transition probability, in which $\mathcal{H}'_1 + \mathcal{H}'_{\text{ex}}$ is taken as a perturbation, gives the relaxation rate for the j th proton that can be written as

$$\frac{1}{T_1^{(3e)}}(j) = \frac{2\pi}{\hbar} (g \mu_B \gamma_N \hbar)^2 G_3(j) I_{3e}. \quad (19)$$

$G_3(j)$ is the same geometrical factor as in the case of the first-order three-magnon process. I_{3e} is a summation over wave vectors and is given by

$$I_{3e} = \frac{3}{16S} N_S^{-3} \sum_{\vec{k}_1} \sum_{\vec{k}_2} \sum_{\vec{k}_3} \frac{\epsilon_m^3}{\epsilon_1 \epsilon_2 \epsilon_3} \{M^2\} [\langle n_1 + 1 \rangle \langle n_2 + 1 \rangle \langle n_3 \rangle \delta(\epsilon_1 + \epsilon_2 - \epsilon_3) + \langle n_1 + 1 \rangle \langle n_2 \rangle \langle n_3 \rangle \delta(\epsilon_1 - \epsilon_2 - \epsilon_3)], \quad (20)$$

where

$$\{M^2\} = \frac{1}{3} \{ [M(\vec{k}_1, \vec{k}_2, \vec{k}_3)]^2 + [M(\vec{k}_2, \vec{k}_3, \vec{k}_1)]^2 + [M(\vec{k}_3, \vec{k}_1, \vec{k}_2)]^2 \} \quad (21)$$

with

$$M(\vec{k}_1, \vec{k}_2, \vec{k}_3) = 4S [J(\vec{k}_1) + J(\vec{k}_2) + J(\vec{k}_3) + J(\vec{k}_1 - \vec{k}_2 - \vec{k}_3) - 2J(\vec{k}_1 - \vec{k}_2) - 2J(\vec{k}_1 - \vec{k}_3)] \epsilon_m / [\epsilon(\vec{k}_1 - \vec{k}_2 - \vec{k}_3)]^2. \quad (22)$$

I_{3e} is different from I_3 by a wave-vector-dependent factor $\{M^2\}$ in the summation. It is rather troublesome to calculate I_{3e} in the nearly-one-dimensional case because we cannot take the angular average as in the isotropic three-dimensional case. We therefore calculated the averages of $\{M^2\}$ numerically for such values of \vec{k}_1 , \vec{k}_2 , and \vec{k}_3 , corresponding to certain sets of energies $\epsilon(\vec{k}_1)$, $\epsilon(\vec{k}_2)$, and $\epsilon(\vec{k}_3)$, that satisfy a δ function. In this way $\{M^2\}$ is calculated as a function of $\epsilon(\vec{k}_1)$ and $\epsilon(\vec{k}_2)$ so that I_{3e} can be reduced to the same double integral that occurs in equation (14b), except for the multiplication by the energy-dependent factor $\{M^2\}$ in the integrand. A typical functional form of $\{M^2\}$ is shown in Fig. 3. The enhancement itself does not diverge for vanishing energy gap as is seen from the low-energy limit of $\{M^2\}$, where the numerator of Eq. (22) is a small quantity of higher order than the denominator which is in agreement with the theory based on the Dyson-Maléev representation.⁹

If the structure contains nonequivalent hydrogen positions, the effective fields at these sites will be different. This will affect the geometrical factor G_i , as it contains the direction of the effective field with respect to the electron-spin-quantization axis and the position of the proton. The temperature-dependent integral I_i , however, is the same for inequivalent protons. From inspection it can be seen that the geometrical factors of the two-magnon and the three-magnon processes are different. Therefore, the ratio of the relaxation rates at inequivalent positions may give an indication of the effective process. The temperature dependence of the relaxation rates is mainly determined by the Bose distribution functions in the integrands of I_2 and I_{3e} . Apart from the numerical values of the relaxation rates, the temperature dependence tends to favor the two-magnon process at low temperatures and the three-magnon process at higher temperatures.

IV. EXPERIMENTAL RESULTS AND DISCUSSION

The measurements reported in this article were performed with an ordinary incoherent, frequency-variable pulsed NMR spectrometer (Matec Model-6600 with homemade timing system). The same single crystals were used as in the steady-state experiments.¹⁵ The spin-lattice relaxation time of the protons was measured by observing the recovery of a free decay or a spin-echo signal, after saturation with a comb of rf pulses. The recovery was exponential over at least one decade. Echo signals in zero applied field were observed in some of the crystals, but the values of T_1 were reproducible. Conventional cryogenic techniques were used to cover a measuring temperature range of 1.1–3.9 K.

The relaxation times for both H(1) and H(2) were measured and the results are shown in Fig. 4. The values of T_1 increase sharply with decreasing temperature. The absolute value of T_1 of H(1)

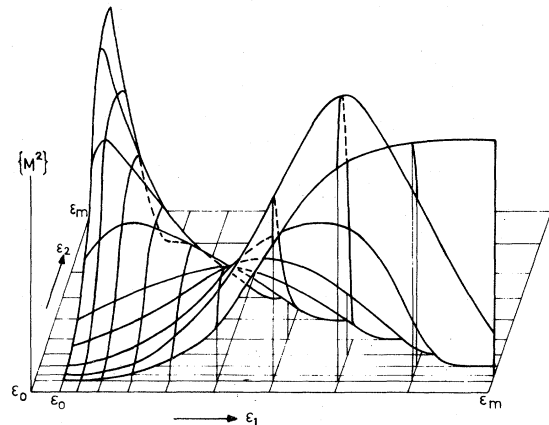


FIG. 3. Typical form of a wave-dependent factor $\{M^2\}$ as a function of $\epsilon(\vec{k}_1)$ and $\epsilon(\vec{k}_2)$.

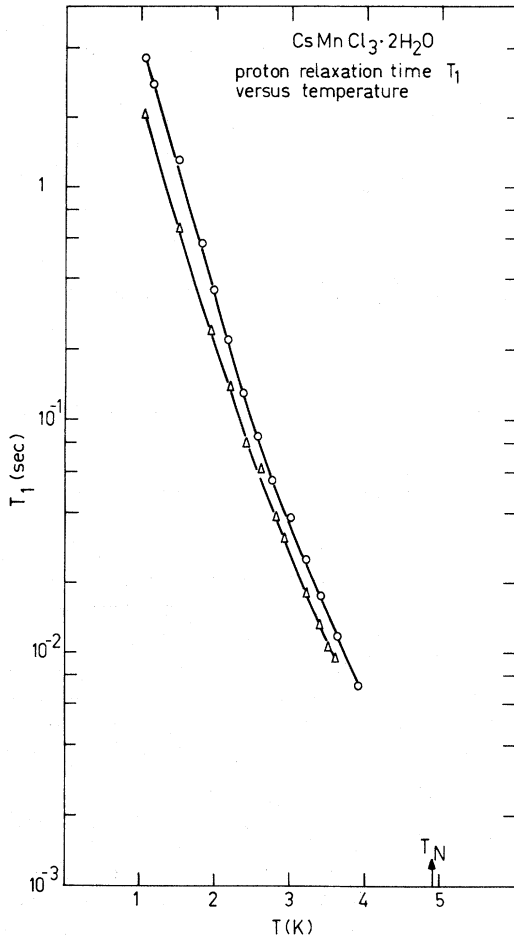


FIG. 4. Experimental spin-lattice relaxation times of H(1) (circles) and H(2) (triangles) versus temperature. The solid lines are "eyeball" fits to the data.

will be discussed later. First, we will sketch experimental trials to assign the relaxation mechanism. The ratio of the measured relaxation rates of H(2) and H(1) is shown in Fig. 5. This ratio must be constant if one relaxation mechanism is dominant in the whole temperature range because the difference of the relaxation rate for H(1) and H(2) originates from the difference in the geometrical factor as discussed before, whereas a change of the positions of the protons with temperature is improbable. Fortunately, the directions of the dipole fields at the sites of H(1) and H(2) are quite different.¹⁵ The calculated ratio of the geometrical factors for the two-magnon process $G_2[H(2)]/G_2[H(1)]$ and for the three-magnon process $G_3[H(2)]/G_3[H(1)]$ are shown in the same figure. These ratios can be considered as the ratios of the relaxation rates for both processes, because both temperature-dependent integrals I_2

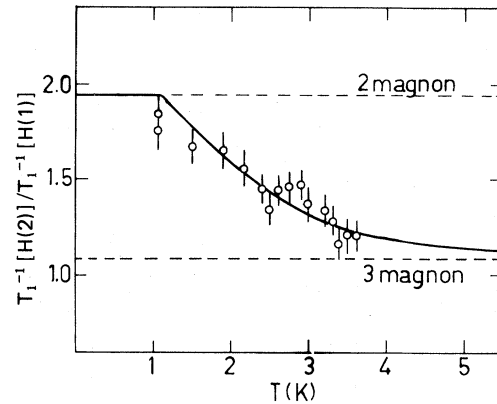


FIG. 5. Ratio of the experimental relaxation rate of H(2) to that of H(1) versus temperature. The calculated ratio of the geometrical factors for the two-magnon process and that of the three-magnon process are also shown with broken lines. The solid line represents the theoretical estimate based on the numerical calculations with $J_1/\kappa = -3.53$ K; $J_2 = 5 \times 10^{-2} J_1$, and $J_3 = 0$.

and I_{3e} are the same for H(1) and H(2). The experimental ratio changes from a value close to the two-magnon value to that close to the three-magnon value with increasing temperature. The drawn curve in Fig. 5 represents an estimate based on numerical calculations, which will be discussed later.

The angular dependence of relaxation rates with changing direction of the applied field were reported in some cases.^{5, 28, 29} In Figs. 6(a) and 6(b) the angular dependence of T^{-1} of proton H(1) is shown for the temperatures 1.50 and 3.21 K. The applied field was rotated in the bc plane and its magnitude was adjusted in order to observe the same resonance line at fixed frequency. In the same figures the angular dependences of the calculated geometrical factors, which are normalized to the values in zero field, are also shown. These figures reveal that the situations are quite different at $T = 1.50$ and 3.21 K. The external field seems to have a strong effect on the spin-wave dispersion and not only on the geometrical factors. These figures, however, indicate that we really are measuring the relaxation time of the proton system and not the relaxation time of the electron spins, because the experimental patterns have no symmetry around the b or c axis.

To simplify the interpretation, we also measured the relaxation rates as a function of the external field in the b direction. We only present data of those symmetry-related protons whose internal fields made the largest angle with this direction, in order to obtain a larger directional change of the total field at the proton site. The effect of the

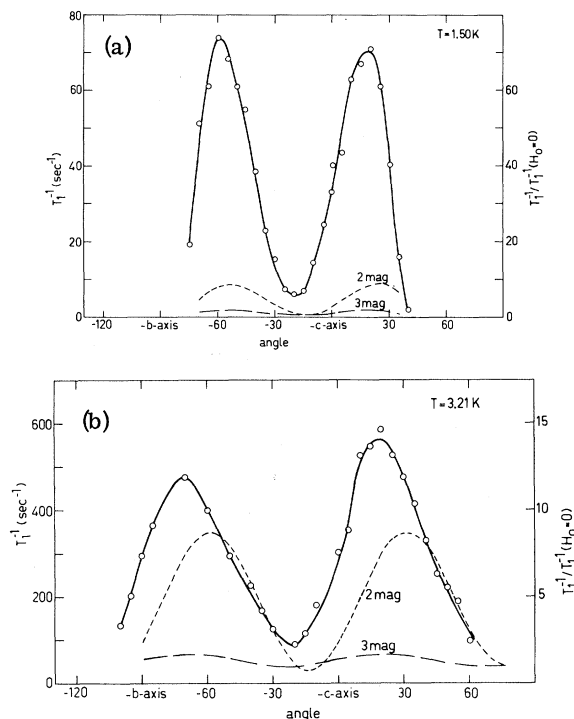


FIG. 6. Angular dependence of the experimental relaxation rates for H(1) at 1.50 K and 10.0 MHz (a), and at 3.21 K and 11.02 MHz (b), where the applied field was rotated in the bc plane. The broken lines show the calculated angular dependence of the geometrical factors which are normalized to the values in zero field (right scale).

external field is only to lower and raise the α , β branches of the spin-wave spectrum. No additional mechanisms have to be considered and the expressions for the geometrical factors (5) and (13) will remain the same. The experimental results of this field dependence for H(1) are shown in Fig. 7. The ratio $T_1^{-1}[\text{H}(2)]/T_1^{-1}[\text{H}(1)]$ is plotted in Figs. 8(a) and 8(b), at the same temperatures as before, together with the calculated field dependence of the ratios of the geometrical factors. The experimental data points are close to the calculated ratio for the two-magnon process at 1.50 K and close to the calculated ratio for the three-magnon process at 3.21 K. This again is a strong indication that the two-magnon process is dominant at low temperatures and the three-magnon process dominates at high temperatures.

Now let us turn to the actual calculation of the relaxation rate as a function of temperature. The geometrical factors are given in Eqs. (5) and (12). The relevant parameters such as the spin structure, the magnitude and direction of the effective field, and the position of the protons were taken

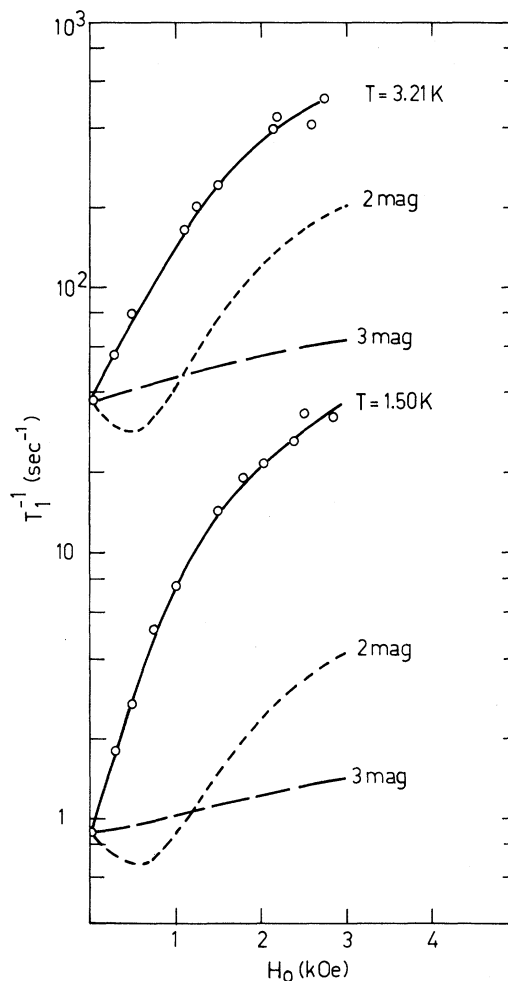


FIG. 7. Field dependence of the experimental relaxation rates for H(1) at 1.50 and 3.21 K, where the direction of the applied field was fixed to the b axis and the operating frequencies were changed. The dotted and broken lines denote the calculated geometrical factors normalized to those in zero field.

from Spence, De Jonge, and Rama Rao.¹⁵ The summation was carried out over 24 Mn^{2+} ions within a distance of 10 \AA from the proton site. The resulting values are

$$G_2[\text{H}(1)] = 1.69 \times 10^{44} \text{ cm}^{-6} \quad (22)$$

and

$$G_3[\text{H}(1)] = 9.02 \times 10^{44} \text{ cm}^{-6}.$$

The temperature-dependent integrals I_2 and I_{3e} are given by Eqs. (6) and (14). The relevant parameters are ϵ_0 , J_1 , J_2 , and J_3 . For ϵ_0 we took the values and temperature dependence quoted by Skalyo *et al.*¹⁶ In Table I several sets of exchange parameters obtained from different experiments

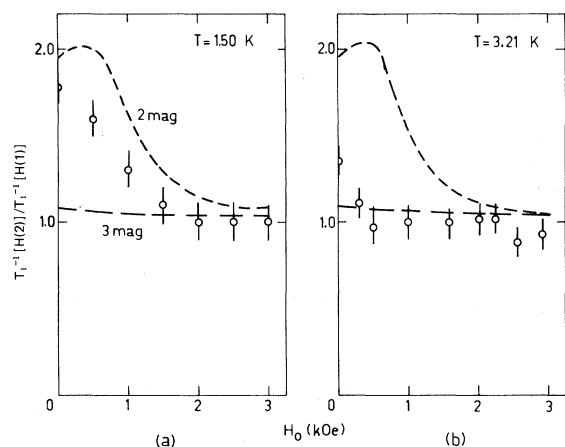


FIG. 8. Field dependence of the ratios of the experimental relaxation rates for H(2) to that of H(1) at 1.50 and at 3.21 K, where the applied field is parallel to the b axis. The calculated ratios of the geometrical factors for the two-magnon and three-magnon processes are also depicted.

are tabulated. For each set of parameters the relaxation time was calculated. Results are shown in Fig. 9. The contributions from the two-magnon process and the exchange-enhanced three-magnon process are plotted separately. Generally, the calculated curves are slightly higher than the experimental data points. However, it should be emphasized that no adjustable parameters have been used in the calculations. In view of this we feel that the agreement with the experimental data is rather satisfactory. Figure 9 also shows that the temperature at which the relaxation rates from the two calculated processes become equal is around 2.5 K for all the different sets of parameters. This fact agrees well with the evidence obtained from the experiments discussed before.

The values for the interchain coupling found in different experiments display a considerable scatter. Probably, however, $J_2 \gg J_3$; a conclusion which agrees with the conjectured relative magnitudes of the interchain coupling based on the crystallographic structure.¹⁷ In view of this, we tried to fit the data with J_2 as an adjustable parameter and $J_1 = -3.53$ K and $J_3 = 0$. A best overall fit on the sum of the two processes was obtained for $J_2 = 5 \times 10^{-2} J_1$. The results of this calculation were also used in the construction of the estimate of the ratio $T_1^{-1}[\text{H}(2)]/T_1^{-1}[\text{H}(1)]$ plotted for comparison in Fig. 5. Also shown in Fig. 9 is the calculated relaxation rate of the first-order three-magnon process for the same set of exchange constants. From the comparison with the exchange-enhanced three-magnon relaxation rate the enhancement factor was found to be approximately

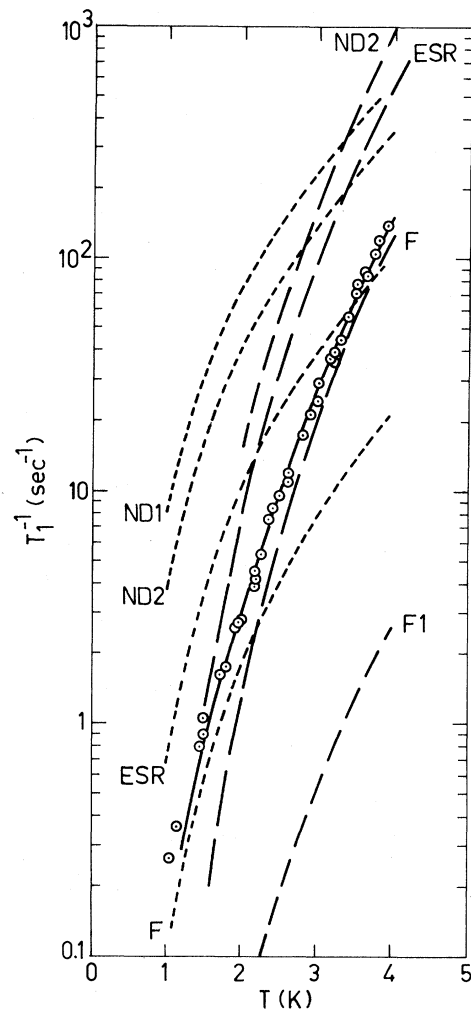


FIG. 9. Examples of the calculated relaxation rates versus temperature for different sets of exchange constants. The dotted lines denote the two-magnon relaxation rates and the broken lines denote rates of the exchange-enhanced three-magnon process. The labels refer to:

$$\text{ND1: } J_1/\kappa = -3.53 \text{ K, } J_2 = J_3 = 0.35 \times 10^{-2} J_1.$$

$$\text{ND2: } J_1/\kappa = -3.53 \text{ K, } J_2 = 0.7 \times 10^{-2} J_1, J_3 = 0.$$

$$\text{ESR: } J_1/\kappa = -3.0 \text{ K, } J_2 = 2.6 \times 10^{-2} J_1, J_3 = 0.$$

$$\text{F: } J_1/\kappa = -3.53 \text{ K, } J_2 = 5 \times 10^{-2} J_1, J_3 = 0.$$

The two sets ND1 and ND2 fit with the neutron-diffraction result (see Table I). ESR is a sample of the range for J_2 and J_3 indicated by line-shape ESR experiments. The values for the exchange constants that result in a best fit to the experimental data points are marked F. The sum of the rates of the two- and three-magnon process for F is denoted with the solid line. The rate of the first-order three-magnon process for F is also shown with the label F1.

40 in this case.

Concluding, we would like to note that, to our knowledge, this is the first example in which the interplay of the two relaxation mechanisms is demonstrated both experimentally and from basic calculations. Experimentally, the use of the ratio of the relaxation rates at nonequivalent nuclei has been shown to be very helpful in the assignment of the effective mechanisms. The calculations showed that, within the framework of existing theory and without adjusting parameters, a satisfactory agreement between experiment and theory could be obtained.

ACKNOWLEDGMENTS

The authors would like to acknowledge Professor P. van der Leeden for his encouraging interest. We thank Dr. C. H. W. Swüste, K. Kopinga, and J. P. A. M. Hijmans for their helpful discussions and for the critical reading of the manuscript. The assistance of M. C. K. Gruyters and J. G. H. M. van Amstel is also gratefully acknowledged. One of the authors (H. N.) wishes to express his deep thanks to the Magnetism Group, Eindhoven University of Technology for their warm hospitality during his stay.

APPENDIX: NUMERICAL CALCULATION OF DENSITY OF STATES OF MAGNON IN $\text{CsMnCl}_3 \cdot 2\text{H}_2\text{O}$

A direct numerical calculation of the surface integral for the density of states (7) is complicated and extremely time consuming. It can also be done by taking a large number of points uniformly in the first Brillouin zone of the \vec{k} space, calculating the energy $\epsilon(\vec{k})$ for each point, and counting the number of points whose energy falls into a certain interval around ϵ .³⁰ This method also takes a long time. We used the following modified way in the case of our spin structure. For fixed k_y, k_z , the distribution of the number of points as a function of ϵ can be written as

$$N(\epsilon, k_y, k_z) = (2/\pi) \epsilon (\epsilon_m^2 - \epsilon^2)^{-1/2} \{ (4S J_1)^2 - [A + (\epsilon_m^2 - \epsilon^2)^{1/2}]^2 \}^{-1/2}, \quad (24)$$

with

$$A = 4S (J_2 \cos \frac{1}{2} k_y c + J_3 \cos k_z b).$$

The density of states $N(\epsilon)$ is now calculated by averaging $N(\epsilon, k_y, k_z)$ over an array of points in the $k_y - k_z$ plane.

- ¹G. E. G. Hardeman, N. J. Poulis, and W. v. d. Lugt, *Physica* **22**, 48 (1956).
²T. Moriya, *Prog. Theor. Phys.* **16**, 23 (1956).
³J. van Kranendonk and M. Bloom, *Physica* **22**, 545 (1956).
⁴T. Oguchi and F. Keffer, *J. Phys. Chem. Solids* **25**, 405 (1964).
⁵N. Kaplan, R. Loudon, V. Jaccarino, H. J. Guggenheim, D. Beeman, and P. A. Pincus, *Phys. Rev. Lett.* **17**, 357 (1966).
⁶P. A. Pincus, *Phys. Rev. Lett.* **16**, 398 (1966).
⁷A. Narath and A. T. Fromhold, Jr., *Phys. Rev. Lett.* **17**, 354 (1966).
⁸D. Beeman and P. A. Pincus, *Phys. Rev.* **166**, 359 (1968).
⁹A. B. Harris, *Phys. Rev.* **183**, 486 (1969).
¹⁰I. J. Lowe and D. W. Whitson, *Phys. Rev. B* **6**, 3262 (1972).
¹¹P. M. Richards, *Phys. Rev. Lett.* **28**, 1646 (1972).
¹²D. Hone, C. Scherer, and F. Borsa, *Phys. Rev. B* **9**, 965 (1974).
¹³S. J. Jensen, P. Andersen, and S. E. Rasmussen, *Acta Chem. Scand.* **16**, 1890 (1962).
¹⁴H. Forstat, J. N. McElearney, and N. D. Love (unpublished).
¹⁵R. D. Spence, W. J. M. de Jonge, and K. V. S. Rama Rao, *J. Chem. Phys.* **51**, 4694 (1969).
¹⁶J. Skalyo, Jr., G. Shirane, S. A. Friedberg, and H. Kobayashi, *Phys. Rev. B* **2**, 4632 (1970); **2**, 1310 (1970).
¹⁷M. J. Hennesy, C. D. McElwee, and P. M. Richards, *Phys. Rev. B* **7**, 930 (1973).
¹⁸F. Borsa and M. Mali, *Phys. Rev. B* **9**, 2215 (1974).
¹⁹F. Ferriou, *Phys. Lett. A* **49**, 253 (1974).
²⁰K. Nagata and Y. Tazuke, *Phys. Lett. A* **31**, 293 (1970).
²¹K. Nagata and Y. Tazuke, *J. Phys. Soc. Jpn.* **32**, 337 (1972).
²²T. Smith and S. A. Friedberg, *Phys. Rev.* **176**, 660 (1968); *Phys. Rev. B* **2**, 781(E) (1970).
²³H. Kobayashi, I. Tsujikawa, and S. A. Friedberg, *J. Low Temp. Phys.* **10**, 621 (1973).
²⁴K. Kopinga, T. de Neef, and W. J. M. de Jonge, *Phys. Rev. B* **11**, 2364 (1975).
²⁵This $|k_1|^2$ is reduced to $\frac{1}{4} F_1(\alpha\beta\gamma)$ in Ref. 2. The value of ϕ is put to zero in Ref. 10, which is not convenient in actual calculation because ϕ_i must be measured with respect to the direction of $\phi = 0$ in that case.
²⁶This functional form differs from Eq. (2.31) in Ref. 2. These approximations have the same functional behavior in the small- k region. Comparison of the resulting relaxation rates will give an indication of the validity of the small- k approximation in the three-dimensional case, because their behavior for larger ϵ is quite different; our form neglects the zone-boundary effect while the form in Ref. 2 usually overestimates this effect.
²⁷T. Oguchi, *Phys. Rev.* **117**, 117 (1960).
²⁸G. E. G. Hardeman, N. J. Poulis, W. v. d. Lugt, and W. P. A. Hass, *Physica* **23**, 907 (1957).
²⁹T. Goto, Y. Ajiro, T. Haseda, H. Nishihara, and A. Hirai, *J. Phys. Soc. Jpn.* **25**, 903 (1968).
³⁰See, for example, J. M. Ziman, *Principles of the Theory of Solids* (Cambridge U. P., London, 1963), Sec. 2.5.